Magnetic Breakdown Effects in the Galvanomagnetic Properties of Zinc*

R. W. STARK†
Department of Physics, Case Institute of Technology, Cleveland, Ohio
and
Department of Physics and Institute for the Study of Metals, University of Chicago, Chicago, Illinois

(Received 6 April 1964)

The galvanomagnetic properties of several single-crystal specimens of high-purity zinc have been investigated. The results of this investigation are presented and a Fermi-surface topology consistent with the data is discussed. Many of the detailed features of the galvanomagnetic properties are found to result from the effects of magnetic breakdown. The open orbit parallel to the hexagonal axis is modified but not eliminated by magnetic breakdown at fields of about 17.5 kG. A "giant orbit" of the type previously observed in magnesium is found in zinc. This orbit results from magnetic breakdown across the energy gap near K which separates the second-band hole sheet from portions of the third-band electron sheets. Magnetic breakdown across this same energy gap gives rise to discrete bands of open trajectories in the basal plane when the direction of the magnetic field is tilted away from the hexagonal axis in the $(10\bar{1}0)$ and $(11\bar{2}0)$ crystallographic planes. The transition region of the magnetic breakdown which gives rise to the giant orbit is investigated in detail, and the large quantum oscillations which have been previously observed in the transport properties of zinc are shown to be a transition-region phenomenon. The oscillations appear to result from an oscillatory breakdown probability which, in turn, arises from oscillations in the density of states associated with the Landau levels of the needle-shaped portion of the Fermi surface of zinc. An analysis of the detailed shape of the oscillations indicates that the Landau levels of the needle are split into discrete spin levels with a very large effective g factor. The three values of the effective g factor which are compatible with the present data are $g^*=90$, $g^*=180$, and $g^*=360$, but an investigation with higher magnetic-field strengths will allow a unique choice to be made. No evidence has yet been obtained that yields a direct confirmation of the quasiparticle states predicted by Pippard.

INTRODUCTION

MUCH experimental and theoretical work has been directed in recent years toward the determination of the electronic band structure of those group II metals which have the hexagonal close-packed crystal structure. Magnesium was the first of these metals to be reasonably well understood. The low-field de Haas–van Alphen measurements of Gordon *et al.*,[1] the pulsed-field de Haas–van Alphen measurements of Priestley,[2,3] and the galvanomagnetic measurements of Stark *et al.*[4,5] have been shown to be in remarkable agreement with Falicov's[6] model for the Fermi surface of magnesium. This model is quite similar to that constructed by Harrison,[7] using the single-orthogonalized plane-wave (OPW) technique for an ideal hexagonal-close-packed divalent metal. Cohen and Falicov have modified Falicov's original model to include the effects of spin-orbit coupling[8,9] and magnetic breakdown.[10] The work in Ref. 5 showed that the galvanomagnetic properties of magnesium were dramatically affected by magnetic breakdown across small energy gaps.

The low-field de Haas–van Alphen measurements of Joseph and Gordon[11] on zinc have shown that, in many respects, the electronic band structure of zinc is similar to that of magnesium if one takes into account the difference in their c/a ratios. This was verified by the magnetoacoustic investigations of Gibbons and Falicov.[12] We were thus led to speculate that perhaps the galvanomagnetic properties of zinc would be similar to those of magnesium, and that since the electronic band structure of these two metals appeared to be similar, one could, in any case, obtain a better understanding of both metals by investigating the galvanomagnetic properties of zinc and comparing them with the galvanomagnetic properties of magnesium. In particular, we hoped to gain a better understanding of the mechanisms of magnetic breakdown.

In addition, we were intrigued by the large amplitude Schubnikov–de Haas oscillations which were observed in the earlier investigations of Borovik[13] and Renton.[14] These oscillations come from the needle portions of the Fermi surface, and are associated with a group of elec-

* Supported in part by the U. S. Air Force Office of Scientific Research and the Advanced Research Projects Agency.

† Present address: Department of Physics and Institute for the Study of Metals, University of Chicago, Chicago, Illinois.

[1] W. L. Gordon, A. S. Joseph, and T. G. Eck, in *The Fermi Surface*, edited by W. A. Harrison and M. B. Webb (John Wiley & Sons, Inc., New York, 1960), p. 84.

[2] M. G. Priestley, Proc. Roy. Soc. (London) **A276**, 258 (1963).

[3] M. G. Priestley, L. M. Falicov, and Gideon Weisz, Phys. Rev. **131**, 617 (1963).

[4] R. W. Stark, T. G. Eck, W. L. Gordon, and F. Moazed, Phys. Rev. Letters **8**, 360 (1962).

[5] R. W. Stark, T. G. Eck, and W. L. Gordon, Phys. Rev. **133**, A441 (1964).

[6] L. M. Falicov, Phil. Trans. Roy. Soc. (London) **A255**, 55 (1962).

[7] W. A. Harrison, Phys. Rev. **118**, 1190 (1960).

[8] M. H. Cohen and L. M. Falicov, Phys. Rev. Letters **5**, 544 (1960).

[9] L. M. Falicov and M. H. Cohen, Phys. Rev. **130**, 92 (1963).

[10] M. H. Cohen and L. M. Falicov, Phys. Rev. Letters **7**, 231 (1961).

[11] A. S. Jospeh and W. L. Gordon, Phys. Rev. **126**, 489 (1962).

[12] D. F. Gibbons and L. M. Falicov, Phil. Mag. **8**, 177 (1963).

[13] E. S. Borovik, Zh. Eksperim. i Teor. Fiz. **30**, 262 (1956) [English transl.: Soviet Phys.—JETP **3**, 243 (1956)].

[14] C. A. Renton, in *Proceedings of the Seventh International Conference on Low Temperature Physics* (University of Toronto Press, Toronto, 1960), p. 153.

trons which represent about one one-millionth of the total charge carriers in zinc. It appeared that a very large fraction of the electrical conductivity resulted from this very minor group of electrons. We hoped to shed some light on the process by which this occurred.

In the preliminary report[15] of this investigation, we showed that the galvanomagnetic properties of zinc are similar to those of magnesium, and, as in magnesium, the striking features resulted from the effects of magnetic breakdown. In particular, the so-called Schubnikov–de Haas oscillations result from a perturbation of magnetic breakdown by the Landau levels of the needle portion of the Fermi surface of zinc.

The preliminary report appeared more or less simultaneously with reports by Alekseevskii and Gaidukov[16] and by Reed and Brennert.[17] All of these reports were in reasonable qualitative agreement, although some disagreement was noted on a few quantitative features. The purpose of this paper is to present the complete results of this investigation and, wherever possible, to illuminate those points on which quantitative disagreement occurred in Refs. 15, 16, and 17.

THEORY OF THE GALVANOMAGNETIC PROPERTIES

The general theoretical interpretation of the galvanomagnetic properties of metal single crystals has been presented in papers by Lifshitz, Azbel, and Kagonov[18] and by Lifshitz and Peschanskii.[19] Their work allows an interpretation of the galvanomagnetic properties of a metal, in the limit of high magnetic-field strength and sample purity, in terms of the topology of its Fermi surface. Alekseevskii *et al.*[20] developed this theory in considerable detail for the specific case of an even valent metal.

The behavior of the galvanomagnetic properties as a function of the type of electronic trajectories that exist for a given direction of the magnetic field H has been elucidated quite thoroughly by these authors for the particular case of transverse magnetoresistance for which H is always held perpendicular to the current density J. This behavior can be summed up by the following four statements:

(1) If, for a specific direction of H, all electron trajectories are closed with $V_1=V_2$, then the resistivity $\rho(\rho=E_{11J}/J$, where E_{11J} is the component of the electric field E measured parallel to the current density J) will be proportional to H^2 in the high-field limit. The definitions of V_1 and V_2 in terms of integrals over the Fermi surface are given in Eq. (25) of Ref. 18. For $V_1=V_2$, the Hall coefficient R is constant but has no simple physical interpretation.

(2) If, for a specific direction of H, all electron trajectories are closed with $V_1\neq V_2$, the resistivity will reach saturation in the high-field limit. For $V_1\neq V_2$, the Hall coefficient R is given by

$$R=h^3/2ec(V_1-V_2).$$

(3) If, for a given direction of H, there exists a layer of open trajectories with a *single* average direction, then in the high-field limit, $\rho=A+BH^2\cos^2\alpha$, where A and B are constants and α is the angle between J and the open trajectory direction in *reciprocal space*. For this case, the Hall coefficient is again constant, but has no simple physical interpretation.

(4) If, for a given direction of H, there exist layers of open trajectories with *different* average directions, the magnetoresistance will saturate in the high-field limit. The Hall "constant" in this case is proportional to $1/H^2$.

These rules can be applied fairly unambiguously as long as the character of the electronic orbits on the Fermi surface does not change as a function of magnetic-field strength. If the basic topology of the Fermi surface changes with changing magnetic-field strength, as may happen when magnetic breakdown occurs, one must be more careful in their application. Reference 5 discusses some of the effects of magnetic breakdown on the galvanomagnetic properties.

The concept of magnetic breakdown was introduced by Cohen and Falicov[10] to explain the presence of the "giant orbit" discovered by Priestley[2,3] in the de Haas–van Alpen effect in magnesium. This concept has been discussed further by Blount[21] and by Pippard.[22,23] The essence of the concept is that when an electron, traveling on one band of the Fermi surface in the presence of a magnetic field, arrives at a Brillouin zone plane at which an energy discontinuity separates the one band of the Fermi surface from a second band of the surface, there is a finite probability that the electron will tunnel through the energy discontinuity and find itself on the second band. The condition for magnetic breakdown is given approximately by $\hbar\omega_c\gg E_g^2/E_F$, where $\hbar\omega_c$ is the Landau level separation, E_g is the band gap, and E_F is the Fermi energy. Pippard has considered a network model for the transition region of magnetic breakdown (the range of magnetic-field strengths for which the probability of an electron jumping the band gap is greater than zero but less than one) and has shown that

[15] R. W. Stark, Phys. Rev. Letters **9**, 482 (1962).
[16] N. E. Alekseevskii and Yu. P. Gaidukov, Zh. Eksperim. i Teor. Fiz. **43**, 2094 (1962) [English transl.: Soviet Phys.—JETP **16**, 1481 (1963)].
[17] W. A. Reed and G. F. Brennert, Phys. Rev. **130**, 565 (1963).
[18] I. M. Lifshitz, M. I. Azbel, and M. I. Kagonov, Zh. Eksperim. i Teor. Fiz. **31**, 63 (1956) [English transl.: Soviet Phys.—JETP **4**, 41 (1957)].
[19] I. M. Lifshitz and V. G. Peschanskii, Zh. Eksperim. i Teor. Fiz. **35**, 1251 (1958) and **38**, 188 (1960) [English transl.: Soviet Phys.—JETP **8**, 875 (1959) and **11**, 137 (1960)].
[20] N. E. Alekseevskii, Yu. P. Gaidukov, I. M. Lifshitz, and V. G. Peschanskii, Zh. Eksperim. i Teor. Fiz. **39**, 1201 (1960) [English transl.: Soviet Phys.—JETP **12**, 837 (1961)].
[21] E. I. Blount, Phys. Rev. **126**, 1636 (1962).
[22] A. B. Pippard, Proc. Roy. Soc. (London) **A270**, 1 (1962).
[23] A. B. Pippard, Phil. Trans. Roy. Soc. (London) (to be published).

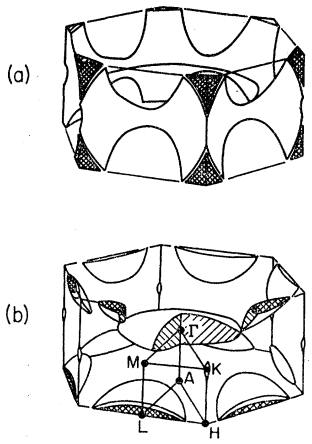

FIG. 1. Single OPW model for the Fermi surface of zinc. (a) First and second bands of holes (first band—"caps"—are shown cross hatched). (b) Third and fourth band of electrons (fourth band—"cigars"—are shown cross hatched). The symmetry points of the hexagonal close-packed Brillouin zone are shown.

in this region there is an entire spectrum of orbits available to the electrons. In particular, there is a finite probability that some of the orbits will be open for magnetic-field strengths in the transition region, regardless of whether any open orbits exist before magnetic breakdown starts or after magnetic breakdown is complete. Thus, one would expect the transition region to be represented in the galvanomagnetic properties by some unusual manifestations. Later in this paper, we will present evidence to show that these manifestations can become quite spectacular.

THE FREE-ELECTRON MODEL FOR THE FERMI SURFACE OF ZINC

Falicov and Cohen[8,9] have shown that the effect of spin-orbit interactions is to cause an essential change in the electronic band structure of metals having the hexagonal-close-packed structure. This change results from the removal of the degeneracy of the energy bands across most of the *AHL* Brillouin zone plane with the result that the double zone scheme usually employed for these metals must be replaced by the conventional single zone scheme. The energy gap that is induced by spin-orbit coupling in zinc is fairly small so that its effects may be neutralized by magnetic breakdown at experimentally attainable magnetic-field strengths.

Harrison's[24] band calculations, the de Haas–van Alphen measurements of Joseph and Gordon,[11] and the magnetoacoustic measurements of Gibbons and Falicov[12] have shown that the free-electron model represents a reasonable first approximation for the Fermi surface of zinc. This model, shown in Fig. 1, consists of separate sheets in the first four Brillouin zones. There is evidence indicating that all six of the pieces shown in Fig. 1 exist. In this paper we will be concerned with only three of these.

The most important sheet of the Fermi surface in its effects on the galvanomagnetic properties of zinc is the multiply-connected second-band hole sheet (the "monster"). This sheet will support a band of open trajectories parallel to the hexagonal axis. The other two sheets of the Fermi surface which have an essential effect on the galvanomagnetic properties are the first-band hole sheets (the "caps") and portions of the third-band electron sheets (the "needles"). Their effect results from magnetic breakdown across the small energy gaps which separate them from the monster. For the first of these, magnetic breakdown across the spin-orbit induced gap between the monster and the caps will eliminate the open orbit parallel to the hexagonal axis while, for the second, magnetic breakdown across the small energy gaps separating the needles from the monster will result in bands of open orbits parallel to the basal plane and the creation of a giant orbit similar to that found in magnesium[2–5,10] when H is nearly parallel to the hexagonal axis.

EXPERIMENTAL TECHNIQUE

The single crystals of zinc which were used in this investigation were grown while the zinc was being purified by zone refining in a helium gas atmosphere.[25] A zone passrate of $\frac{1}{2}$ in. per h resulted in nearly perfect single crystals with less than 0.02° of random microstructure as determined by x-ray measurements. The starting stock had a residual resistance ratio (rrr $=\rho_{300°K}/\rho_{0°K}$, where $\rho_{0°K}$ is the resistivity extrapolated to 0°K) of about 4000. After 15 zone passes, the rrr increased to about 25 000, and after 40 zone passes, the rrr was 50 000.

The individual single-crystal specimens were cut from the bulk single crystals with an acid string saw after the bulk crystals had been oriented using standard x-ray techniques. The specimens, whose average dimensions were 0.060 in.$\times$0.070 in.$\times$0.650 in., were normally cut to within $\pm\frac{1}{3}°$ of a desired crystallographic direction, although extreme care was needed for certain specimen orientations, which we will discuss later, to ensure that the accuracy of orientation was better than $\pm$0.1°. Current and potential leads were soldered directly to the specimen with a contact area at the potential junction of about 3×10^{-4} sq in. The specimen was then suspended vertically in a liquid-helium bath between the pole faces of a dc electromagnet that could be rotated in the horizontal plane. A constant current of about 1.0 A was passed through the specimen, and the potential between a given set of potential leads was continuously monitored as the magnetic field of constant strength was rotated at 20° per min. The transverse magnetoresistance voltage typically varied from about 10^{-6} to 10^{-3} V compared with a noise background of 1.5×10^{-9} V.

All of the transverse magnetoresistance data presented in this paper has been normalized by dividing the specimen's resistance measured in the presence of a

[24] W. A. Harrison, Phys. Rev. **126**, 497 (1962).

[25] We would like to thank J. Friar and P. M. Everett for their assistance in preparing the zinc specimens.

magnetic field by its resistance measured when $H=0$, since this ratio is independent of the geometry of the individual specimens. The zero-field resistance of the specimens is normally measured in the same cryostat in which the galvanomagnetic measurements are made. However, we found that the residual field of our magnet (about 70 G) was almost sufficient to double the value of the specimen's resistance. Thus, we measured the zero-field resistance of each of the specimens in a storage Dewar away from the residual fringe field of the magnet. These measurements were made with an accuracy of $\pm 2.5\%$.

THE DIRECTIONS OF H WHICH PRODUCE OPEN TRAJECTORIES IN ZINC

Of the four types of behavior for the transverse magnetoresistance discussed in the theory section, the data obtained in this investigation showed regions of types 1, 2, and 3, but no evidence was found for a type 4 region. Regions of type 1 behavior (all closed trajectories and $V_1=V_2$) were found to be predominant as expected since zinc is an even valent metal. The only region of type 2 behavior found (all closed trajectories and $V_1\neq V_2$) occurred when H was parallel to the hexagonal axis.

Figure 2 is a stereographic projection of those directions of H in reciprocal space for which the transverse magnetoresistance exhibits type 3 behavior (open trajectories with a single average direction). Directions of H will be given by the coordinates θ, the angle between H and b_3, and ϕ, the angle between the plane of H and b_3 and the plane of b_1 and b_3. Current directions will be designated by θ' and ϕ' defined in the same manner. The crosses in Fig. 2 show the current directions of some of the specimens investigated.

The periphery of the stereogram (H parallel to the basal plane) is a one-dimensional type 3 region with open trajectories parallel to b_3. The circular region

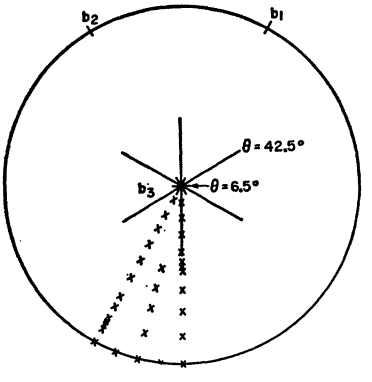

FIG. 2. Stereogram of the magnetic-field directions which give rise to bands of open trajectories in zinc. b_1, b_2, and b_3 are the basis vectors of the hexagonal reciprocal lattice. b_1 and b_2 are oriented in ΓM directions, 60° apart, relative to the Brillouin zone shown in Fig. 1. b_3 is parallel to ΓA. The pole of the stereogram is along the sixfold b_3 axis. The crosses show the current directions of some of the specimens investigated.

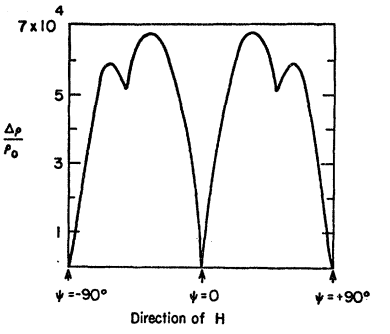

FIG. 3. Transverse magnetoresistance rotation diagram for J in the $\phi'=180°$; $\theta'=90°$ direction. ψ is the angle between the plane of H and J and the plane of J and b_3. The transverse magnetoresistance saturates at $\psi=0°$ and at $\psi=\pm 90°$ but varies as H^2 elsewhere.

about the pole of the stereogram ($\theta \lesssim 1.3°$) is a two-dimensional type 3 region with open trajectories having a net direction parallel to the basal plane. The radial lines about the pole are one-dimensional regions with open trajectories directed perpendicular to the plane represented by the radial line. Thus, this stereogram is in essence the same as that found for magnesium,[5] and the topology of the Fermi surface of zinc must be equivalent to that of magnesium.

We will consider first the experimental evidence which indicates the existence of the band of open trajectories parallel to b_3. Until quite recently, the data pertinent to these trajectories have contained sufficient ambiguity as to cast doubt on their existence in magnetic field strengths above a few kG.[26] The ambiguity arose from an apparent inability to obtain saturation of the transverse magnetoresistance when J was nearly perpendicular to the direction of the band of open trajectories in reciprocal space (cf. Fig. 4, Ref. 17). Figure 3 is a transverse magnetoresistance rotation diagram for J in the $\theta'=90°$; $\phi'=180°$ direction (for this specimen J makes an angle of $90°\pm 0.1°$ with the open trajectory parallel to b_3). The sharp minima at $\psi=0°$ and at $\psi=\pm 90°$ occur when H is parallel to b_3 and to the basal plane, respectively. We have found that the behavior of the transverse magnetoresistance at $\psi=\pm 90°$ is extremely sensitive to the relative orientation of J with respect to the basal plane. If J deviates from the basal plane by more than 0.1°, or if the crystal is warped by more than 0.1°,[27] it is impossible to observe satura-

[26] This open orbit has recently been observed in the magnetoacoustic effect in zinc by B. C. Deaton and J. D. Gavenda (private communication).

[27] Early in this investigation we attempted to obtain accurate orientation of J in the basal plane by cleaving a sample from a large single crystal of zinc, since zinc cleaves in the basal plane. However, we found that when we cleaved a sample thin enough for our purposes we no longer had a basal plane but had instead a basal "surface" since cleaving warped the crystal. The typical warp which we observed was about 0.1° per mm of sample width in the basal plane. The effect of this warping is to average the magnetoresistance over magnetic-field directions within a few tenths of degrees of the basal plane or around the bottom and sides of the very sharp minima at $\psi=\pm 90°$ in Fig. 3, yielding a fairly large H^2 contribution at the minimum rather than saturation.

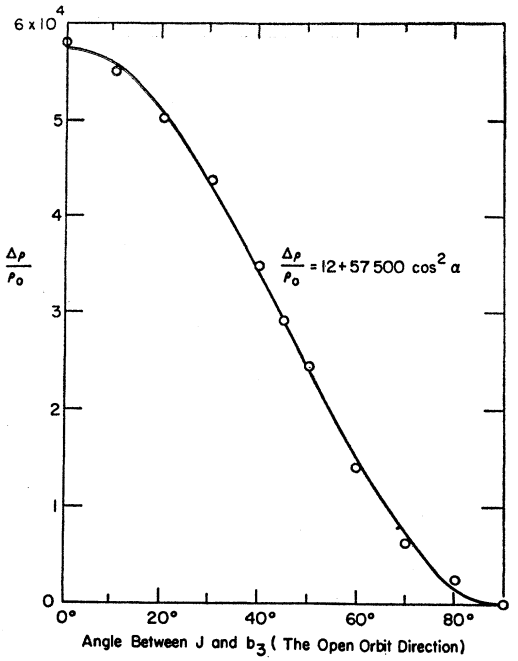

FIG. 4. Current "rotation" diagram for H in the $\phi=30°$; $\theta=90°$ direction. The data were taken with $H=23$ kG.

tion in this minimum. We observed saturation here (curve 1, Fig. 5) only by taking extreme care in the orientation and handling of this specimen.

Figure 4 shows a "current" rotation diagram for H in the $\theta=90°$; $\phi=30°$ direction. This diagram was plotted by selecting data from the transverse magnetoresistance rotation diagrams for the appropriate directions of H and J. The solid curve, which fits the data quite well, has the form

$$\Delta\rho/\rho_0=12+108\ (\mathrm{kG})^{-2}H^2\cos^2\alpha,$$

where α is the angle between J and b_3. This is the form of the transverse magnetoresistance for type 3 behavior when α measures the angle between J and the open trajectory direction in reciprocal space. Thus, this direction of H produces a band of open trajectories parallel to b_3.

Figure 5 shows a log-log plot of the magnetoresistance as a function of magnetic-field strength for two directions of J when H is in the $\theta=90°$; $\phi=30°$ direction. Curve 1 is from a specimen with J accurately perpendicular ($\theta'=90°\pm0.1°$; $\phi'=180°$) to the open trajectory direction along b_3. The transverse magnetoresistance saturates for this specimen, but a definite change in the rate of saturation occurs at about 17.5 kG. After the change occurs, the transverse magnetoresistance tends to saturate more quickly than before. Curve 2 is for a specimen with J in the $\theta'=87°$; $\phi'=180°$ direction. Here, the transverse magnetoresistance is proportional to H^2 below 17.5 kG, changes slope rapidly at about 17.5 kG, and rises at a rate considerably below H^2 above the transition field strength.[28] This transition at 17.5 kG is typical of the behavior for other directions of J when H is in the basal plane and must result from the onset of magnetic breakdown of the spin-orbit coupling induced energy gap between the second-band monster and the first-band caps. We will discuss this breakdown in more detail later.

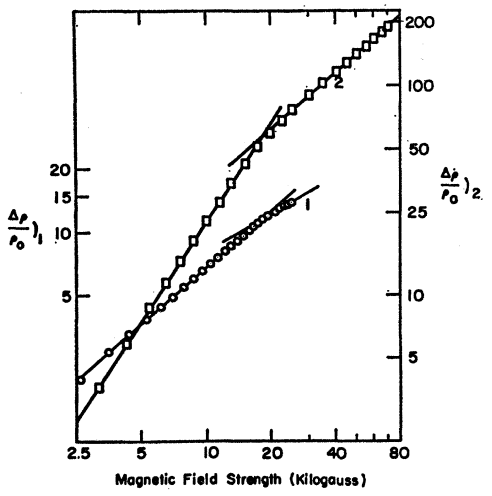

FIG. 5. The transverse magnetoresistance as a function of magnetic-field strength for H in the $\phi=30°$; $\theta=90°$ direction. Curve (1) shows the saturating component of the open orbit magnetoresistance. Curve (2) shows the $BH^2\cos^9\alpha$ component of the open orbit magnetoresistance. The change in slope at 17.5 kG results from the effects of magnetic breakdown. The open orbit is parallel to b_3.

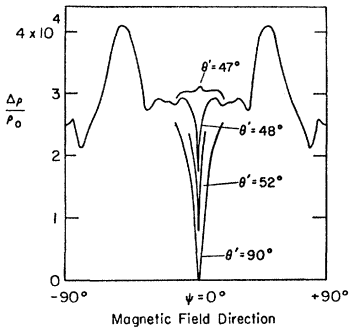

FIG. 6. Portions of transverse magnetoresistance rotation diagrams for different directions of J in the $\phi'=210°$ plane. The sharp minima occurs when H, J, and b_3 are coplanar.

We will consider next the experimental evidence supporting the existence of the bands of open trajectories associated with the longer of the sets of radial lines on the stereogram in Fig. 2 (lines of the type labeled $\theta=42.5°$). Figure 6 shows portions of transverse magnetoresistance rotation diagrams for various directions of J in the $\phi'=210°$ plane. The angle ψ is measured between the plane of H and J and the plane of J and b_3. The sharp minima at $\psi=0°$ thus occur when H, J, and b_3 are coplanar. The transverse magnetoresistance saturates at $\psi=0°$ for $\theta'\gtrsim55°$, but does not saturate

[28] We would like to thank G. V. Brown for permission to publish the data shown in curve 2. G. V. Brown, M. S. thesis, Case Institute of Technology, 1963 (unpublished).

for $\theta' \lesssim 55°$, although the characteristic minima extends to $\theta' = 48°$. This behavior as discussed in Ref. 5 results when the size of the band of open trajectories approaches zero as H approaches a type 1 region where the transverse magnetoresistance varies as H^2. Thus, this band of open trajectories disappears between $\theta' = 48°$ and $\theta' = 47°$, or approximately at $\theta' = 47.5°$ (the equivalent magnetic-field direction is $\phi = 30°$; $\theta = 42.5°$).

Figure 7 shows current "rotation" diagrams for various directions of H along the radial line in the $\phi = 30°$ plane. Curves of the type $\Delta\rho/\rho_0 = A + B\cos^2\alpha$ fit the data quite well when α is measured from the $\phi = 120°$; $\theta = 90°$ direction. Thus, these directions of H must give rise to a band of open trajectories whose direction of propagation is perpendicular to the $\phi = 30°$ plane.

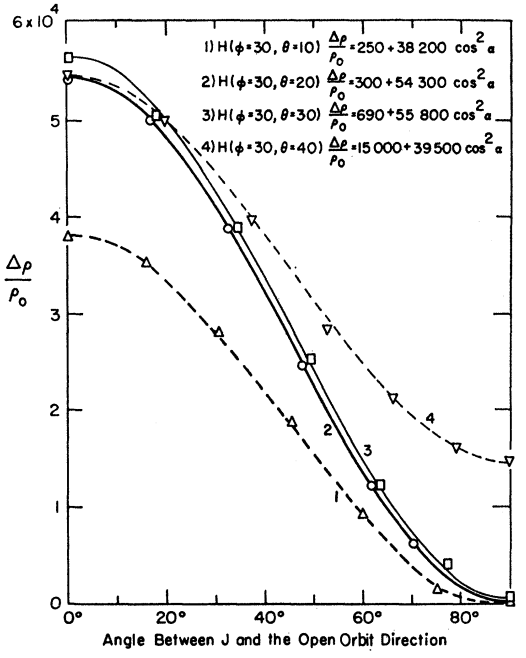

FIG. 7. Current rotation diagrams for four different directions of H in the $\phi = 30°$ plane. H, J, and b_3 are coplanar at 90°. The data were taken with $H = 23$ kG.

An alternate measurement can be made to determine the length of these radial lines. Figure 8 shows a transverse-to-longitudinal rotation diagram for J in the $\phi' = 210°$; $\theta' = 90°$ direction and H in the plane of J and b_3. The normal transverse magnetoresistance value is obtained when H is parallel to b_3 at 0° in Fig. 8. The minima at $\pm 90°$ occur when H is parallel to J. As H is moved from b_3 toward J, it sweeps along one of the longer radial lines in Fig. 2 producing an open trajectory perpendicular to J. The magnetoresistance saturates until H approaches the end of the radial line, where it increases rapidly as the size of the band of open trajectories approaches zero, forming a smooth but definite transition as H enters the type 1 region at the end of the radial line. The length of the line, measured from b_3,

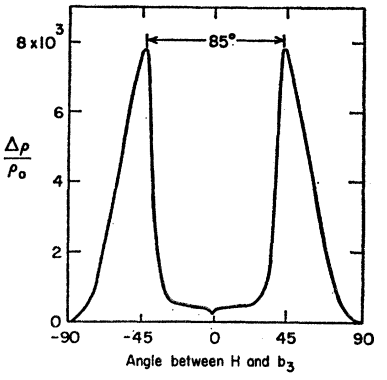

FIG. 8. Transverse-to-longitudinal magnetoresistance rotation diagram for J in the $\phi' = 210°$; $\theta' = 90°$ direction with H, J, and b_3 always coplanar. The transverse magnetoresistance saturates at 90° when H is parallel to J. The broad valley around 0° results from a band of open trajectories propagating perpendicular to the plane of H, J, and b_3.

is given by one-half the distance between the transition peaks of Fig. 8 or $\theta = 42.5°$, in accord with that discussed above.

The length of the shorter set of radial lines shown in Fig. 2 has been determined in a fashion similar to that described above. The transverse magnetoresistance saturated when H, J, and b_3 were coplanar with J in the $\phi' = 180°$ plane for $\theta' \gtrsim 84°$. The characteristic sharp minima which had been associated with the saturating magnetoresistance disappeared at $\theta' \simeq 84°$, setting the length of these lines at $\theta \simeq 6°$. A more accurate determination has been obtained from the transverse-to-longitudinal rotation diagrams shown in Figs. 9(a) and 9(b) for J parallel to b_3 and H in the $\phi = 0°$ plane. The minimum around 0° in Fig. 9(a) occurs when H is almost parallel to J. Figure 9(b) shows the details of this minimum. The magnetoresistance drops very rapidly, suffers a sharp transition, remains nearly constant at $\Delta\rho/\rho_0 \simeq 5$ for 13°, and then rises very rapidly. The magnetoresistance rotation diagram near this minimum changed its character quite drastically with

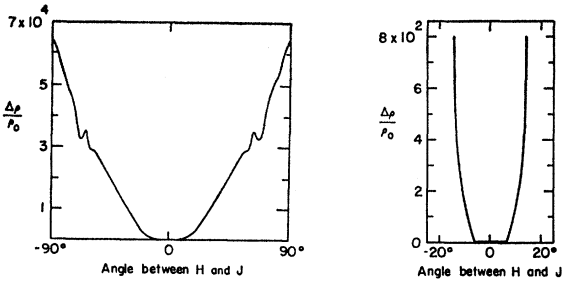

FIG. 9. (a) Transverse-to-longitudinal magnetoresistance rotation diagram for J in the $\theta' = 0°$ direction, with H in the $\phi = 0°$ plane. H is parallel to J at 0°. (b) Detail of the magnetoresistance minimum near 0°. After the sharp transition, the magnetoresistance is nearly constant with variations which are less than the thickness of the curve.

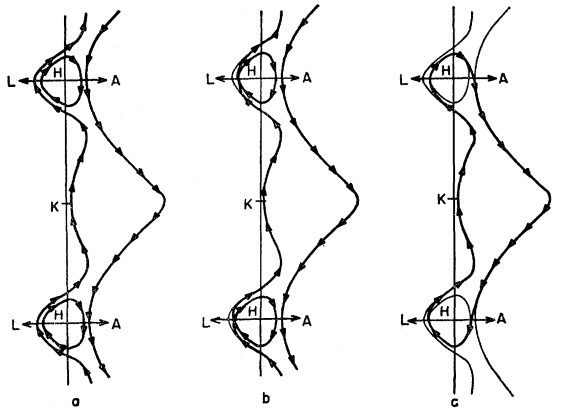

FIG. 10. (a) Cross section of the "monster" and "cap" showing the trajectories on these portions of the Fermi surface before magnetic breakdown of the spin-orbit coupling induced energy gap across the AHL plane. (b) Cross section showing a possible trajectory if the energy gap between H and L is broken down while the energy gap between H and A is not broken down. (c) Cross section showing the trajectory when the spin-orbit coupling induced energy gap in the AHL plane is completely broken down.

minor changes in the position of the specimen with respect to the plane of rotation of H. If the specimen was tilted about its length by more than 5 min of arc, the flat bottom in the rotation diagram disappeared; if the tilt was larger than 0.5°, the minimum was replaced by a small but fairly sharp local maximum. The flat bottom shown in Fig. 9(b) occurs when H accurately traverses the short radial line. The length of this line measured from b_3 is 6.5°.

The size of the two-dimensional region about b_3 was determined from a transverse-to-longitudinal rotation diagram for J in the $\phi'=195°$; $\theta'=90°$ direction and H in the $\phi=15°$ plane. Again, the character of the magnetoresistance was extremely sensitive to the absolute orientation of H in this plane, but careful measurements showed that the two-dimensional region more or less formed a circle of 1.3° in diameter about b_3. This region, together with the two sets of radial lines discussed above, results from magnetic breakdown in and near the ΓKM plane of the Brillouin zone between the second-band monster and the third-band needles.

INTERPRETATION OF THE OPEN TRAJECTORIES

The information contained in the stereogram shown in Fig. 2 can be interpreted in terms of the single OPW model for the Fermi surface of zinc as described earlier if one includes the possibility of magnetic breakdown across small energy gaps. In the absence of magnetic breakdown, the effect of spin-orbit coupling is to remove the degeneracy of the energy bands across most of the AHL Brillouin zone plane with the result that the monster becomes multiply connected and supports a band of open trajectories parallel to b_3, whenever H is parallel to the basal plane. When the evidence for this open orbit was discussed earlier, we pointed out that the transverse magnetoresistance goes through a fairly sharp transition around 17.5 kG. This transition must be associated with the onset of magnetic breakdown across the spin-orbit coupling induced energy gap in the AHL plane, but the evidence indicates that the breakdown may proceed in a rather surprising fashion.

The most puzzling aspect of the transition is that the saturating component of the transverse magnetoresistance (curve 1, Fig. 5) for this open orbit tends to saturate more quickly or at a lower value after the transition than before. One would expect the transverse magnetoresistance to vary as H^2 after this orbit has been completely lost, and that the initial change in the behavior of the magnetoresistance with the onset of breakdown would be a departure from rather than a closer approach to saturation. This behavior seems to indicate an increase in the number of open trajectories with a resulting increase in the quantity V_1-V_2 for the closed orbits remaining. This is consistent with the behavior of the Hall field for this same specimen.

Our other measurements have indicated, however, that an increase in the size of the band of open trajectories leads to an increase in the $BH^2\cos^2\alpha$ component of the resistivity associated with the open trajectory. Curve 2 of Fig. 5 shows that, in this particular case, the H^2 component of the resistivity suffers a decrease above 17.5 kG, as if the size of the band of open trajectories had been decreased. We believe that the apparently contradictory behavior of these two curves can be explained by the effects of partial magnetic breakdown.

Figures 10(a), (b), and (c) show cross sections of the monster and cap in the reduced zone scheme for H parallel to ΓM. The arrows indicate the electron trajectories on the surface. The spin-orbit coupling induced energy gap in the AHL plane separates the cap from the monster with the result that the electron trajectories on the monster are open and the trajectories on the cap are closed as shown in Fig. 10(a). Since the induced energy gap is small, one would expect magnetic breakdown to eventually eliminate its effects and cause the monster and cap to form a combined surface. If this happened, the trajectory would be that shown in Fig. 10(c). However, we do not know the exact size of the energy gap or the exact fashion in which it varies over the AHL

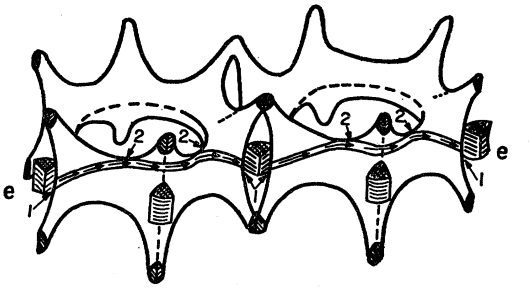

FIG. 11. A perspective drawing of the monster and needle sheets of the Fermi surface showing a band of the *ee* open trajectories.

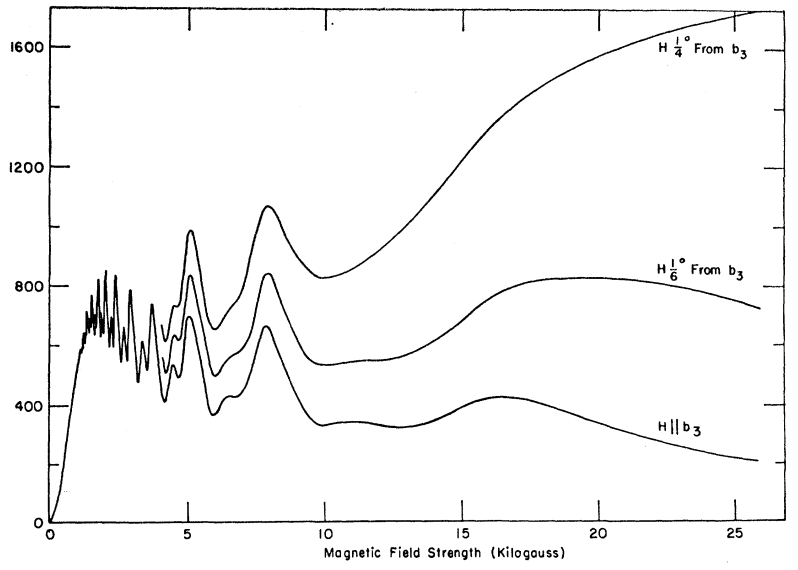

FIG. 12. The "transverse" magnetoresistance as a function of the magnitude of H for J in the $\phi'=210°$; $\theta'=90°$ direction. The three curves show how rapidly the magnetoresistance changes in the minimum at $\psi=0°$ in Fig. 3 when the plane of rotation of H is not exactly perpendicular to J. This dependence is a unique feature of magnetic-field directions nearly parallel to b_3.

plane. We do know that the size of the gap is extremal at H, approaches zero as one goes from H to A or from H to L, and remains zero along the entire AL line.[8,9] Thus, since the contact area of the monster tentacle with the AHL plane is fairly large, one would expect a reasonable variation in this plane of the size of the energy gap between the monster and cap. If this were the case, then for a given magnetic-field strength, magnetic breakdown could become highly probable over portions of the AHL plane while remaining highly improbable over other portions. Such a situation is shown in Fig. 10(b). We have assumed for the sake of argument that the energy gap approaches zero more rapidly along HL than along HA, and that the probability of jumping the gap along HL for a given magnetic-field strength is high, while the probability of jumping the gap along HA is small. The effect of this would be twofold. First, the closed orbits around the cap would disappear as these become incorporated in the band of open trajectories. This would increase the quantity V_1-V_2 for closed orbits and might explain curve 1 of Fig. 5. Second, the path length traveled during one period of the open trajectory would increase with a resulting increase in the time necessary to repeat one period. This would cause an effective decrease in $\omega\tau$ for this orbit and could explain curve 2 of Fig. 5.

All of the remaining sets of open trajectories, as well as the type 2 region parallel to b_3, can be explained by magnetic breakdown across the small energy gaps near K which separate the monster from the needles. Magnetic breakdown at this point is, in essence, identical with that observed in magnesium and leads to results more or less identical in the galvanomagnetic properties. These results have been discussed in detail in Ref. 5.

The longer radial lines ($\theta=42.5°$) on the stereogram shown in Fig. 2 result from the *ee* band of open trajectories shown in Fig. 10(a) in Ref. 5. These arise when H is tilted from b_3 in planes of the type $\phi=30°$. The *ee* bands of open trajectories pass through regions of breakdown, miss regions of breakdown, pass through regions of breakdown, etc., and have a net direction perpendicular to the plane containing H and b_3. The short radial lines ($\theta=6.5°$) result from the *ff* band of open trajectories shown in Fig. 10(b) in Ref. 5. These arise when H is tilted from b_3 in planes of the type $\phi=0°$. The two-dimensional region about $b_3(\theta\lesssim 1.3°)$ is also caused by this breakdown. While the *ee* and *ff* open trajectories are periodic in passing through and above regions of breakdown, and are propagated along the major crystallographic directions in the basal plane, the ones generated within the two-dimensional region are in general aperiodic.

Figure 11 is a perspective drawing of the monster in an extended zone scheme. Also shown are those portions of the needles which were found to be in contact with the monster via magnetic breakdown near point K for magnetic-field strengths of 26 kG. A band of the *ee* open trajectories is shown on the surface for H tilted approximately 35° from b_3 in the $\phi=30°$ plane. Reference 5 showed that the two points on the combined surface which limit the thickness of the band of open trajectories are point 1 on Fig. 11, the lowest point where magnetic breakdown occurs, and point 2, the minimum height of the monster waist (both are measured parallel to b_3).

Reference 5 also showed that an analysis of the geometry of the *ee* and *ff* open orbits allows one to determine the vertical separation between points 1 and 2 of Fig. 11 and the horizontal distance of point 2 from the center of the Brillouin zone. These two lengths are $\frac{1}{2}(h_b+h_w)$ and L. h_b is the length measured parallel to b_3 of the region of magnetic breakdown, h_w is the mini

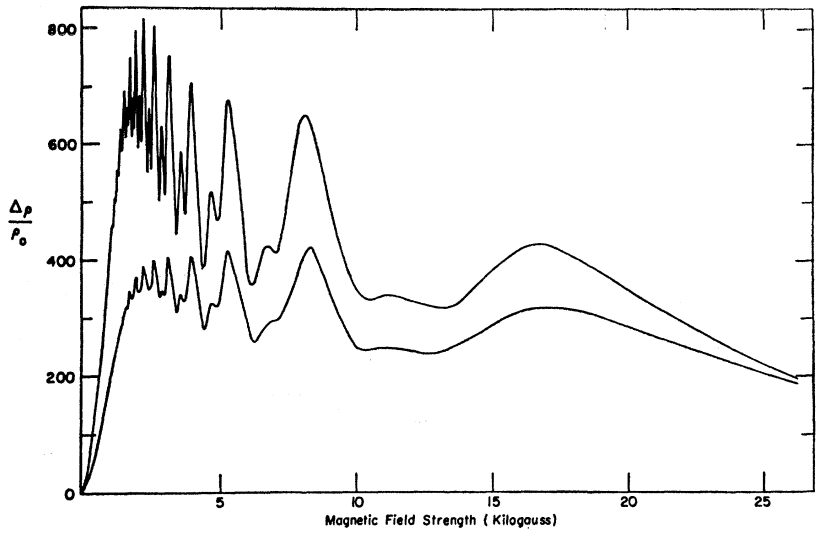

FIG. 13. Transverse magnetoresistance as a function of magnetic-field strength for J in the $\phi'=210°$; $\theta'=90°$ direction and H within 0.01° of b_3. Both curves were taken from the same specimen. The lower curve was obtained at 4.2°K and the upper curve was obtained at 1.6°K. The difference between these two curves results from an increase in the average relaxation time at 1.6°K by a factor of 1.56 from that at 4.2°K. The quantum oscillations result from a perturbation of magnetic breakdown. ρ_0 for the lower curve is 1.80×10^{-10} Ω-cm, and ρ_0 for the upper curve is 1.15×10^{-10} Ω-cm.

mum thickness measured parallel to b_3 of the monster waist, and L is the distance from Γ to the projection of point 2 on the basal plane. The results are

$$\tfrac{1}{2}(h_b+h_w)=0.12\ \text{Å}^{-1},$$
$$L=1.05\ \text{Å}^{-1}.$$

This value of L is quite consistent with the single-OPW model for the Fermi surface of zinc.

THE GALVANOMAGNETIC PROPERTIES FOR H PARALLEL TO b_3

The only type 2 region (all closed trajectories and $V_1\neq V_2$) observed in this investigtaion occurred for the isolated direction of H parallel to b_3. For this field direction, the transverse magnetoresistance saturated independently of the direction of J. However, the behavior at saturation changed drastically if H deviated slightly from b_3. Figure 12 shows the variation of the transverse magnetoresistance as a function of the magnitude of H for H nearly parallel to b_3 with J in the $\phi'=210°$; $\theta'=90°$ direction. The deviations noted in Fig. 12 are measured for H in the plane of J and b_3; they are *not* measured for H in the plane perpendicular to J, i.e., the normal plane of rotation of H. Note that if H deviates by as little as 0.25° from b_3 in the J b_3 plane the magnitude of the transverse magnetoresistance for $H=25$ kG is increased tenfold from its value when H is accurately parallel to b_3. This extreme sensitivity on the absolute orientation of H is typical of that discussed earlier and led us to develop a scheme for orienting these crystals in a magnetic field with an accuracy of ±0.01° relative to b_3.

First, we found that our standard fixed crystal holders, to which the crystal was held with a small spring loaded clamp, could reproducibly locate the crystal in the magnetic field with an accuracy of only ±0.75°. Then we tried attaching the crystal to various rotating mounts with which adjustments could be made while the crystal was in the cryostat, but these located the crystal with a reproducible accuracy that was no better than ±0.2°. The problem was finally solved by locking a fixed crystal holder into the tail of the cryostat and tilting the entire cryostat. This resulted in a 4-ft lever arm whose displacement was measured with a micrometer, allowing angle measurement with a reproducible accuracy of 0.01°.

Figure 13 shows the transverse magnetoresistance as a function of magnetic field strength for J in the $\phi'=210°$; $\theta'=90°\pm0.1°$ direction and H within 0.01° of b_3. The two curves shown were taken at two different temperatures. The lower curve was taken at $T=4.2$°K while the upper was taken at $T=1.6$°K. The difference between the two curves arises primarily from the fact that the specimen's resistivity was limited by electron-phonon interactions at 4.2°K. The resistivity ratio at 4.2°K ($R_{300°K}/R_{4.2°K}$) was 32 000, whereas the ratio at 1.6°K ($R_{300°K}/R_{1.6°K}$) had risen to 50 000. These curves have two predominant features. The first is the large amplitude oscillatory component which is periodic in H^{-1}. The period of these oscillations is identical to the de Haas–van Alphen period of the needle-shaped portion of the Fermi surface. The second predominant feature is the pronounced humping, especially of the upper curve, at about 2.5 kG. Both of these features, as well as the fact that the transverse magnetoresistance does saturate, result from the effects of magnetic breakdown. In the course of this discussion, we hope to shed some light on the manner in which these effects are produced. At present, it is sufficient to say that they both occur in the transition region of magnetic breakdown.

Figure 14 shows a basal plane cross section of the monster and needles, together with the trajectories which exist on these sheets of the Fermi surface when H is parallel to b_3. Orbits of the kind labeled 1 and 2 exist for magnetic-field strengths sufficiently small that

the energy gaps at points "a" are not broken down. When the probability of magnetic breakdown becomes equal to one, the 1 and 2 orbits disappear and are replaced by 3, the giant orbit. Pippard[23] has shown that in the transition region, where the probability of breakdown across the gap "a" is greater than zero but less than one, all three of the above orbits exist simultaneously, together with an entire spectrum of other possible trajectories, including some open trajectories which can propagate in any direction in the basal plane. It is magnetic breakdown across the gaps "a" that is responsible for the behavior of the transverse magnetoresistance curves shown in Fig. 13.

One of the transition region effects of magnetic breakdown is to broaden the Landau levels. Pippard has considered intralevel transitions which can occur in the broadened levels and has shown that such transitions lead to nonlocalized Bloch-type states (called quasiparticles in Ref. 23), which react to an applied electric field in the same manner that a free electron would react in the absence of a magnetic field. These quasiparticles make a significantly different contribution to the elements of the conductivity tensor than do the electrons involved in interband transitions. When $\omega_c\tau\gg1$, the quasiparticle contribution to the element σ_{11} of the conductivity tensor will be given by $\sigma_{11_q}=a_1(H)\tau_q$. However, the quasiparticles will not contribute to σ_{12}. On the other hand, the electrons involved in those interband transitions which lead to *closed* orbits will contribute to both σ_{11} and σ_{12}. Their contribution to σ_{11} is given by $\sigma_{11_c}=a_2(H)/H^2\tau$, and their contribution to σ_{12} is given by $\sigma_{12_c}=a_3(H)$. The fact that $a_1(H)$, $a_2(H)$, and $a_3(H)$ are all functions of the magnitude of H indicates their functional dependence on the probability of magnetic breakdown which in turn is a function of the magnitude of H.

One other group of electrons may make a significant contribution to σ_{11} but not to σ_{12}. These electrons are involved in interband transitions leading to nonperiodic trajectories which can propagate in random directions in the basal plane. These arise by chance in the transition regions, and we are particularly interested in those which propagate through several different zones in reciprocal space. These trajectories are basically random, and it seems reasonable to give them the properties of a random walk. If this is the case, their contribution to σ_{11} will be given by $\sigma_{11_r}=a_4(H)\tau^{1/2}$.

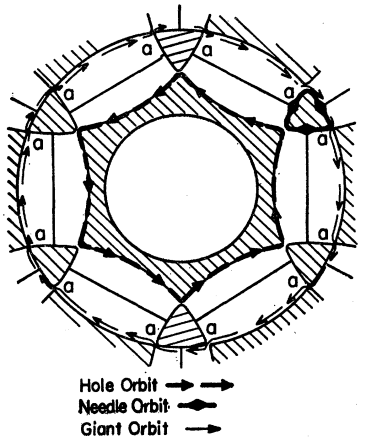

FIG. 14. Basal plane cross section (not to scale) of the monster and needle sheets of the Fermi surface of zinc showing the orbits which exist before and after magnetic breakdown of the energy gaps at points "a."

The two types of interband transitions discussed above can be characterized by the same relaxation time τ. However, it is not at all apparent that the quasiparticle relaxation time will be the same, so we have characterized it separately as τ_q. Since the contributions to the conductivities are additive, σ_{11} and σ_{12} are given by

$$\sigma_{11}=a_1(H)\tau_q+a_2(H)/H^2\tau+a_4(H)\tau^{1/2}, \quad (1)$$

$$\sigma_{12}=a_3(H), \quad (2)$$

when $\omega_c\tau\gg1$. It is worth noting that σ_{12} is determined solely by interband transitions leading to closed orbits.

It is apparent then that the transition region of magnetic breakdown will be characterized by three intrinscially different types of electronic states. We cannot easily determine their relative importance on the basis of existing theory. We can, however, obtain some information by considering the experimental data. The experiment involves measuring the elements of the resistivity tensor which must be reciprocated to obtain the conductivity tensor to compare with theory. When H is parallel to b_3, the resistivity and conductivity tensors are isotropic in the basal plane,[29] and the elements, σ_{11} and σ_{12}, of the conductivity tensor are related to the elements, ρ_{11} and ρ_{12}, of the resistivity tensor by

$$\sigma_{11}=\rho_{11}/(\rho_{11}^2+\rho_{12}^2), \quad (3)$$

$$\sigma_{12}=\rho_{12}/(\rho_{11}^2+\rho_{12}^2), \quad (4)$$

[29] In general, the resistivity tensor $\tilde{\rho}$ has the form

$$\tilde{\rho}=\begin{pmatrix}\rho_{11} & \rho_{12} & \rho_{13}\\ \rho_{21} & \rho_{22} & \rho_{23}\\ \rho_{31} & \rho_{32} & \rho_{33}\end{pmatrix},$$

where the elements ρ_{ij} can, in principle, contain terms which are both even and odd functions of **H**. If we place **H** along a symmetry direction, we can usually reduce the tensor by performing symmetry operations about **H**. We need only note that **H** has the properties of an axial vector as contrasted with **E** and **J**, which are polar vectors.

If $\tilde{S}$ is a symmetry operation about **H** which leaves the properties of the crystal invariant, then this can be applied to the general expression for Ohm's law.

$$\mathbf{E}=\tilde{\rho}\mathbf{J}$$

to yield

$$\tilde{S}\mathbf{E}=\tilde{S}\tilde{\rho}\mathbf{J}=\tilde{S}\tilde{\rho}\tilde{S}^{-1}\tilde{S}\mathbf{J},$$

but both E and J must be left invariant by the symmetry transformation, i.e.,

$$\mathbf{E}=\tilde{S}\mathbf{E},$$
$$\mathbf{J}=\tilde{S}\mathbf{J},$$

so that

$$\tilde{\rho}=\tilde{S}\tilde{\rho}\tilde{S}^{-1}.$$

For the case which we are considering here, H is parallel to a sixfold crystallographic axis. Applying the appropriate symmetry operations reduce the resistivity tensor to the form

$$\tilde{\rho}=\begin{pmatrix}\rho_{11} & \rho_{12} & 0\\ -\rho_{12} & \rho_{11} & 0\\ 0 & 0 & \rho_{33}\end{pmatrix}.$$

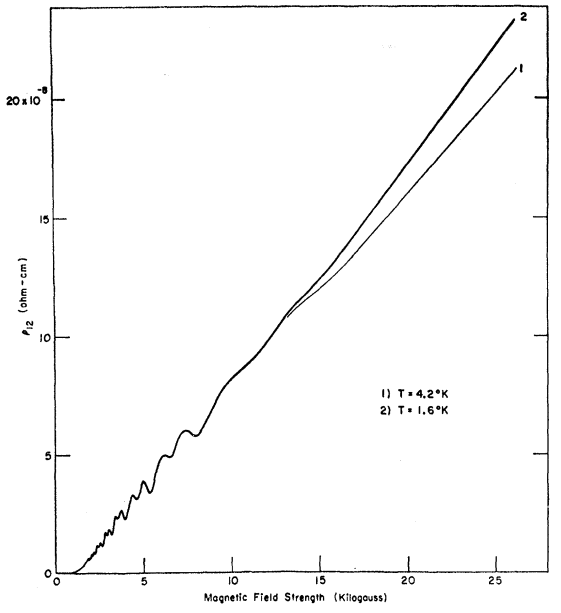

FIG. 15. Hall resistivity ρ_{12} as a function of magnetic-field strength for J in the $\phi'=210°$; $\theta'=90°$ direction and H within 0.01° of b_3. The data were obtained at 4.2 and 1.6°K.

where ρ_{11} is the transverse magnetoresistivity and ρ_{12} is the Hall resistivity.

ρ_{11} as a function of magnetic-field strength for J in the $\phi'=210°$; $\theta'=90°\pm0.1°$ direction and H within 0.01° of b_3 can be obtained from the data in Fig. 13 by multiplying the plot of $\Delta\rho/\rho_0$ by the given value of ρ_0. ρ_{11} is then shown for two different temperatures, 4.2 and 1.6°K. The remainder of the data to be discussed in this section was taken with this same specimen during the same run and at these same two temperatures. For this specimen, we estimate that $\omega_c\tau\simeq15$ at 4.2°K and $\omega_c\tau\simeq25$ at 1.6°K when $H=1$ kG. Thus, we are certainly in the region needed to satisfy Eqs. (1) and (2) when $H\gtrsim2$ kG.

Figure 15 shows the variation of ρ_{12} with magnetic-field strength. Curve 1, taken at 4.2°K, is shown for $H\gtrsim14$ kG. Curve 1 is nearly the same as curve 2 (taken at 1.6°K) in the lower field region where most of the oscillations occur. The only significant difference is that the amplitude of the oscillations is about 10% smaller at 4.2°K than at 1.6°K. The sign of ρ_{12} is characteristic of excess electrons. ρ_{12} is essentially equal to zero for $H\lesssim1$ kG.

The data shown in Figs. 13 and 15 were used to obtain σ_{11} and σ_{12} from Eqs. (3) and (4). We will consider σ_{12} first since, according to Eq. (2), this element of the conductivity tensor contains only the contribution arising from those interband transitions leading to closed orbits. It is convenient to plot the quantity

$$\Delta N=\sigma_{12}H/2ec \tag{5}$$

instead of σ_{12}, since ΔN contains more intrinsic information than σ_{12} alone. Figure 16 shows ΔN as a function of magnetic-field strength at 4.2 and at 1.6°K. There are several noteworthy features about these curves. First, with the exception of the amplitude of the oscillatory component, ΔN appears to be independent of temperature, and hence independent of τ, since τ is about 1.5 times larger at 1.6°K than at 4.2°K. This is strictly in accord with Eq. (2). Second, one notes a general increase in ΔN with increasing H starting from $\Delta N\simeq0$ at $H=1$ kG. This increase is associated with increasing magnetic breakdown which apparently does not become significant until $H\simeq1$ kG. The third feature to be noted on these curves is the large amplitude oscillatory component of ΔN. For the present, we will ignore the secondary structure in these oscillations and consider only their gross features.

These oscillations which are periodic in H^{-1} have the de Haas–van Alphen period of the needle portion of the Fermi surface. However, the needle is a very tiny portion of the Fermi surface and is capable of containing only about 10^{16} electrons/cm³. A typical oscillation in ΔN has an amplitude of about 10^{21} electrons/cm³ or about 10^5 times more electrons/cm³ than can be contained in the needles. Thus, it is quite apparent that these are not Schubnikov–de Haas oscillations, but are, indeed, oscillations in the magnetic breakdown. They result from the fact that the magnitude of the transmission probability for magnetic breakdown depends on the relative density of states of equal energy in the two bands between which magnetic breakdown occurs. In the absence of an applied magnetic field, the density of states can be considered to form a continuum as a function of the k vector. The presence of a magnetic field, however, quantizes the electrons' angular momentum, creating discrete, highly degenerate energy levels about which the density of states may be sharply localized. Any fluctuation in the density of states will

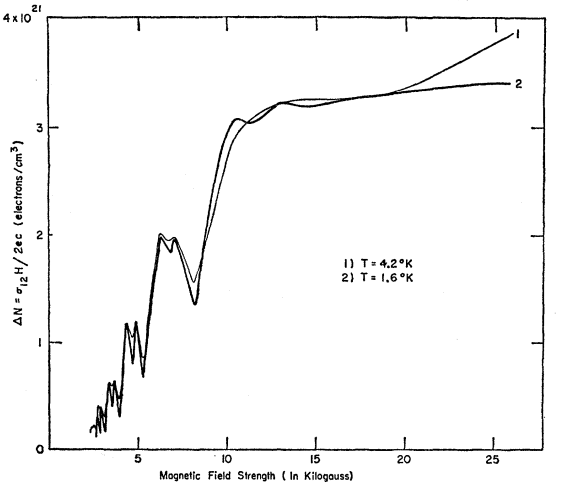

FIG. 16. Plot of ΔN as a function of magnetic-field strength. The increase and oscillations in ΔN reflect the increase and oscillations in the magnetic breakdown probability.

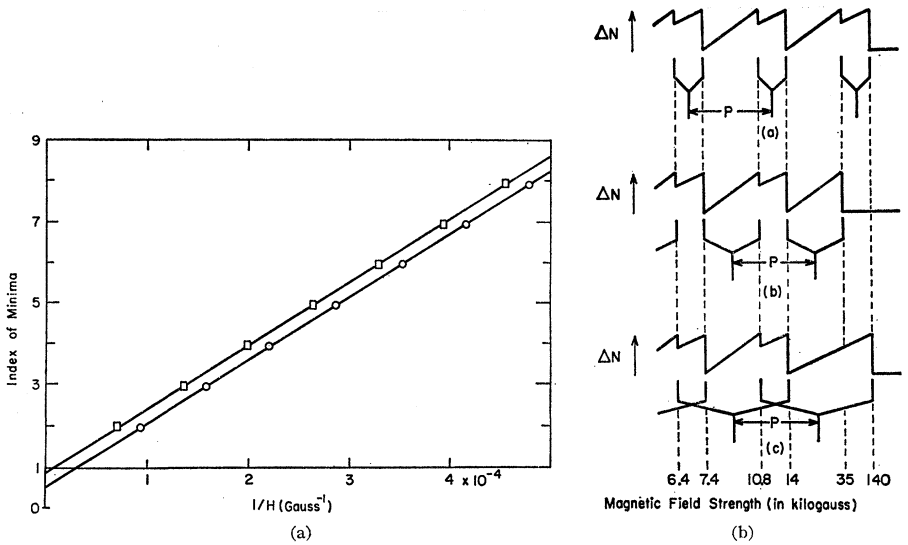

FIG. 17. (a) Period plot of H^{-1} of the maxima in the oscillations of ΔN, a portion of which are shown in Fig. 16. This plot, showing one of the three possible ways in which the maxima can be indexed, is associated with type (a) splitting shown in Fig. 17(b). (b) The three possible ways in which the original Landau levels of the *needle* can be split into discrete spin levels by the effects of spin-orbit coupling. The oscillatory structure that one would expect to observe in ΔN for each of these splittings is also shown. The data allow us to eliminate all other possibilities.

cause a fluctuation in the transmission probability and hence a fluctuation in ΔN. Since the Landau levels pass through the Fermi level periodically in H^{-1}, the density of states at the Fermi level will oscillate periodically in H^{-1}, causing a periodic oscillation in the transmission probability, and finally a periodic oscillation in ΔN. A maximum in ΔN corresponds to a maximum in the transmission probability which occurs when a Landau level is at the Fermi surface.

The amplitude of these oscillations will, among other things, depend on the energy spacing of the Landau levels. This spacing is given by

$$\Delta\epsilon=\hbar\omega=\hbar eH/m^*c. \tag{6}$$

For a particular value of H, $\Delta\epsilon$, for a given band, depends only on the electrons' effective mass m^* in the band. The effective mass of the electrons on the needle is particularly small when H is parallel to b_3 with $m^*_N=0.0075m_0$,[30] where m_0 is the free-electron mass. The energy spacing $\Delta\epsilon_N$ of the electrons on the needle is $\Delta\epsilon_N=0.0075$ eV for $H=5$ kG. This is of the same order of magnitude as the energy gap across which magnetic breakdown is occurring. Thus, it is not surprising that the Landau levels of the needle cause a significant perturbation in the magnetic breakdown. The energy spacing of the Landau levels of the monster is less than $\frac{1}{2}\%$ of $\Delta\epsilon_N$ and does not produce a noticeable perturbation. Thus, for our discussion, we can consider that magnetic breakdown takes place between a first band (the monster) in which the density of states form a continuum and a second band (the needles) in which the density of states is well localized about the Landau levels.

It becomes apparent, then, that the oscillations in ΔN are a direct reflection of oscillations in the density of states of the needle. The fine structure of the oscillations in ΔN must reflect the fine structure in the density of states. Note that each major peak of ΔN in Fig. 16 is split into two distinctly separate maxima. Figure 17(a) shows a period plot in H^{-1} for these maxima. The points occur pair-wise and fall along two parallel lines with a period of $P=6.42\times10^{-5}$ G^{-1}. Thus, each pair of maxima must correspond to one original Landau level that has been split into two discrete spin levels by the effects of spin-orbit coupling. One should note that the indexing of these maxima is not unique. There are two other possible ways in which they could have been indexed.

Figure 17(b) shows the three possible ways in which the original Landau levels can be split into discrete spin levels. Also shown is the basic structure which one would expect to observe in the oscillations of ΔN, for these splittings. The energy equation $E=(n+\gamma\pm\delta)\hbar\omega$ and effective g factor for each of these splittings is given below.

(a) $E_a=(n+0.30\pm\frac{1}{6})\hbar\omega$, $g^*_a=90$,

(b) $E_b=(n+0.80\pm\frac{1}{3})\hbar\omega$, $g^*_b=180$,

(c) $E_c=(n+0.80\pm\frac{2}{3})\hbar\omega$, $g^*_c=360$.

Measurements to higher fields will be necessary before a unique choice can be made. Type (a) splitting will have maxima at 35 and 140 kG; type (b) will have a maximum only at 35 kG, and type (c) will have a maximum only at 140 kG. Thus, measurements to about 40 kG will be sufficient at least to reduce the number of possiblities. If a maximum is observed at 35 kG, type (c) splitting will be eliminated. If no maximum is observed at 35 kG, both (a) and (b) will be eliminated, with type (c) being left as the unique choice.

Effective g factors of the magnitude listed above have been observed previously in semiconductors and semimetals, but none have been observed to our knowledge which differed appreciably from a value of 2 in any metal with a large number of conduction electrons.

[30] F. T. Hedgcock and W. B. Muir, Phys. Rev. **129**, 2045 (1963).

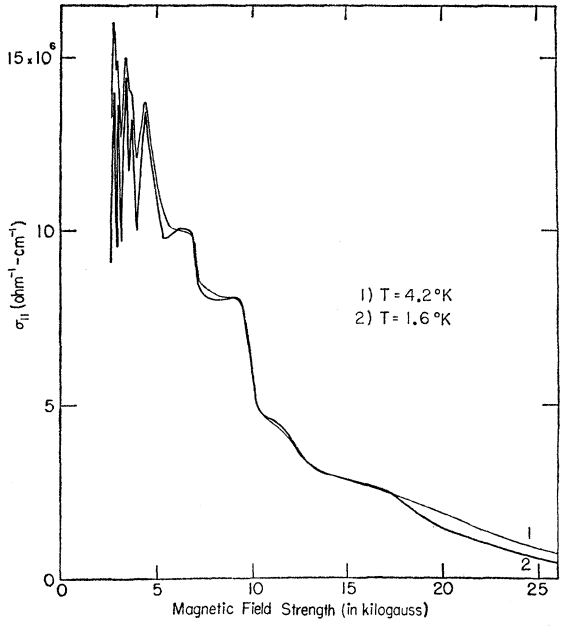

FIG. 18. Plot of σ_{11} as a function of magnetic-field strength for J in the $\phi'=210°$; $\theta'=90°$ direction and H within 0.01° of b_3. The data were taken at 4.2 and 1.6°K.

These large values for g^* are not surprising, however, since Cohen and Blount[31] have shown that Fermi surface sheets split off by small band gaps, and on which the electrons have small effective masses will, in general, have large effective g factors. These conditions are just those which arise in the needle in zinc.

Thus, analysis of σ_{12}, or more appropriately ΔN, yields a considerable amount of information not only about the details of magnetic breakdown but also about the Landau levels of the needle. It should be noted that although the maxima of ΔN shown in Fig. 16 are independent of temperature, the minima are much deeper at 1.6° than at 4.2°K. This probably results from the fact that the density of states is more sharply localized about the Landau levels at 1.6° than at 4.2°K due to a decrease in collision broadening associated with an increase in τ.

The effects observed in σ_{12} are due to interband transitions leading to closed orbits. We must now look at σ_{11} to see what information can be obtained about other types of electronic transitions associated with magnetic breakdown. Figure 18 shows σ_{11} as a function of magnetic-field strength at 4.2 and at 1.6°K. The two curves are somewhat separated for $H\lesssim 5$ kG, almost identical for 5 kG$\lesssim H\lesssim$17 kG, and again separated for $H\gtrsim 17$ kG. The oscillations in σ_{11} are fairly sharp for $H\lesssim 5$ kG and show some sharp secondary structure for $H\lesssim 4$ kG. However, they become quite unimpressive and lose all secondary structure for $H\gtrsim 5$ kG. The amplitude of the oscillations for $H\gtrsim 5$ kG is approximately 5% of the magnitude of σ_{11} for a given value of H. We believe that these oscillations in σ_{11} can be explained by the oscillations in ΔN discussed previously.

The information that is available on the Fermi surface of zinc suggests that it contains about 10^{22} each of electrons and holes per cm³. The component of σ_{11} due to closed trajectories, i.e., $a_2(H)/H^2\tau$, is proportional to the total number of the electrons, plus holes per cm³. The difference between the number of electrons and holes is ΔN, shown in Fig. 16. A typical oscillation in ΔN has an amplitude of about 10^{21} electrons per cm³, or about 5% of the total number of electrons, plus holes per cm³. Thus, a typical oscillation in $a_2(H)/H^2\tau$ will have an amplitude of about 5% of its total value. This is just about sufficient to explain the amplitude of oscillation observed in σ_{11} for $H\gtrsim 5$ kG. It appears, then, that the oscillations in the galvanomagnetic properties discussed in this section can be attributed to interband transitions leading to closed trajectories when $H\gtrsim 5$ kG.

The sharp oscillations which occur in σ_{11} for $H\lesssim 5$ kG cannot be explained by the oscillations in ΔN. These must arise from one of the other contributing terms in σ_{11} listed in Eq. (1). However, we do not have sufficient information at this time to determine whether they are associated with interband transitions leading to nonperiodic trajectories which can propagate in random directions in the basal plane [contributing a term, $a_4(H)\tau^{1/2}$ to σ_{11}], or whether they are associated with quasiparticles [contributing a term, $a_1(H)\tau_q$ to σ_{11}]. The only pertinent information available is the fact that the sharp secondary oscillations in σ_{11} retain the same periodicity and phase for $H\lesssim 5$ kG that they have for $H\gtrsim 5$ kG where we have shown that they result from spin-splitting of the original Landau levels of the needle. Thus, the secondary structure in σ_{11} for $H\lesssim 5$ kG most certainly arises from this same spin-splitting and suggests that oscillations in the transmission probability associated with oscillations in the density of states are

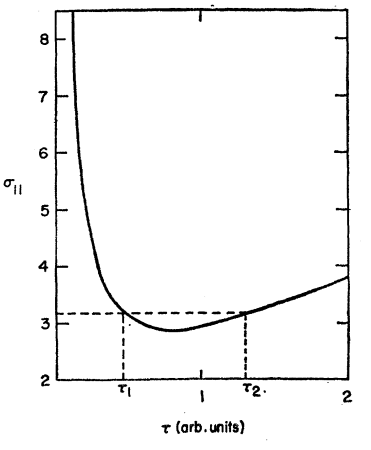

FIG. 19. Plot of the equation $\sigma_{11}=a_1(H)\tau_q+a_2(H)/H^2\tau+a_4(H)\tau^{1/2}$ as a function of τ for the case in which $a_1(H)=a_2(H)/H^2=a_4(H)=1$ and $\tau_q=\tau$. This shows the unusual manner in which σ_{11} may vary with τ in the transition region of magnetic breakdown.

[31] M. H. Cohen and E. I. Blount, Phil. Mag. 5, 115 (1960).

responsible for the structure of the oscillations for $H \lesssim 5$ kG, as well as for $H \gtrsim 5$ kG. This could cause oscillations in both the interband and quasiparticle contributions to σ_{11}. Thus, further investigations will have to be completed before this question can be resolved.

Another detail of the curves shown in Fig. 18 that is worth noting is the fact that σ_{11} is essentially independent of temperature for 5 kG$\lesssim H \lesssim$17 kG. This is rather remarkable since the average electronic relaxation time at 1.6°K is about 1.5 times larger than the relaxation time at 4.2°K. If the interband transitions leading to closed orbits dominated σ_{11}, one would expect σ_{11} to vary as τ^{-1} for a given value of H. This suggests that other contributions to σ_{11} are still important in this region, and that one should study σ_{11} as a function of τ for constant magnetic-field strengths in order to determine the relative importance of the various contributions. Figure 19 shows a plot of Eq. (1) as a function of τ for a given set of values for $a_1(H)$, $a_2(H)$, and $a_4(H)$. Note that σ_{11} has a minimum with respect to τ, and that for certain values of τ, such as τ_1 and τ_2 on Fig. 19, σ_{11} would appear to be independent of τ. An investigation of σ_{11} as a function of τ is being carried out at present and will be the subject of a future report.

COMMENTS ON THE FERMI SURFACE OF ZINC

We have sufficient information at the present time to make some fairly definite statements about the Fermi surface of zinc. The plot of ΔN as a function of magnetic-field strength shown in Fig. 16 shows that ΔN becomes nearly independent of magnetic-field strength with a value of about 3.3×10^{21} electrons/cm^3 for $H \gtrsim 10$ kG. This suggests that magnetic breakdown is nearly complete, and that most of the orbits in the breakdown region are giant orbits. Reference 5 showed that when this is the case, the height of the region of giant orbits h_g, measured parallel to b_3, can be calculated quite simply from the value of ΔN associated with the giant orbits. This yields a value of $h_g = 0.075$ Å^{-1}, which must then be equal to the smaller of the two heights h_b and h_w. h_b is the height of the region of magnetic breakdown and h_w is the caliper of the monster waist in the ΓALM plane, both measured parallel to b_3. This value of h_g must be equal to h_b since it is too small to be consistent with what is known about the size of the monster waist. It we use this together with the sum:

$$\tfrac{1}{2}(h_b+h_w)=0.12 \text{ Å}^{-1}$$

obtained earlier by analyzing the stereographic projection of magnetic-field directions which give rise to open trajectories, we obtain a value for h_w of

$$h_w=0.17 \text{ Å}^{-1}.$$

This dimension is a little less than one-half that of the single OPW model for the Fermi surface of zinc, and is consistent with the de Haas–van Alphen data of Joseph and Gordon. The length of the needle h_n as obtained from the data of Ref. 11 by assuming that the needle is an ellipsoid of revolution is

$$h_n=0.22 \text{ Å}^{-1},$$

compared with the single OPW value of 0.35 Å^{-1}. Thus, h_b is smaller than both h_w and h_n.

If the energy gap between the needle and the monster were sufficiently small that magnetic breakdown occurred along the entire length of the needle, one would expect h_b to be equal to h_w. However, at 25 kG, h_b is less than half of h_w, and the variation of ΔN indicates that h_b is increasing very slowly at a rate of about 1×10^{-3} Å^{-1} per kG. Thus, we are led to believe that the energy gap between the needles and the monster must increase very rapidly as one moves from K toward H along the needle. The rate of divergence may be as large as 3 eV per Å^{-1} at 0.04 Å^{-1} above the ΓKM plane. This rate of divergence was calculated assuming that the energy gap was constant at about 0.01 eV over the entire range of 0.075 Å^{-1} found to be broken down at 12 kG. Although this rate of divergence seems to be exceptionally large, it is substantiated by the de Haas–van Alphen data of Joseph and Gordon.

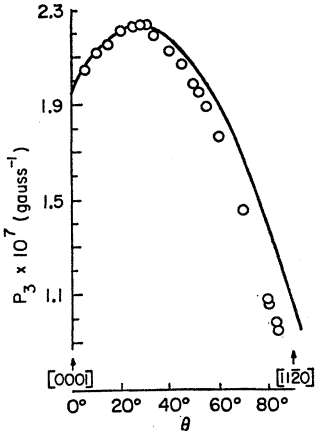

FIG. 20. The variation of "P_3" as a function of θ for H in the $\phi=30°$ plane. P_3 is the de Haas–van Alphen period associated with the vertical tentacles of the monster. These data were published by Joseph and Gordon in their report on the low-field de Haas–van Alphen effect in zinc (Ref. 11).

Figure 20 shows the angular variation of "P_3," one of the set of periods observed by Joseph and Gordon. This period arises from the vertical tentacles of the monster. The minimum cross section of the monster arm that is observed is about two-thirds smaller than that predicted by the single OPW model. The solid curve is the angular dependence of a cylindrical surface with a minimum cross section of 0.0426 Å^{-2} and a cylinder axis tilted 28.5° from [0001] toward [11$\bar{2}$0]. The data points do not deviate very much from cylindrical behavior. The deviations that exist indicate that the surface is slightly hyperboloidal. The remarkable feature of these data is that this period can be followed to within 7° of the [11$\bar{2}$0] direction. This does not appear to be compatible with the single OPW model. However, a minor modification of the single OPW model produces a surface that fits the data quite well.

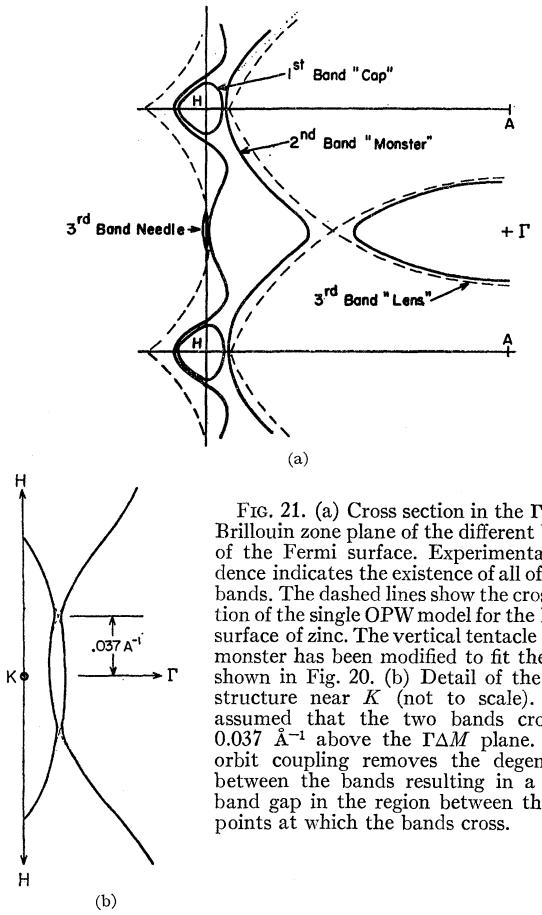

FIG. 21. (a) Cross section in the ΓAHK Brillouin zone plane of the different bands of the Fermi surface. Experimental evidence indicates the existence of all of these bands. The dashed lines show the cross section of the single OPW model for the Fermi surface of zinc. The vertical tentacle of the monster has been modified to fit the data shown in Fig. 20. (b) Detail of the band structure near K (not to scale). It is assumed that the two bands cross at 0.037 Å^{-1} above the $\Gamma\Delta M$ plane. Spin-orbit coupling removes the degeneracy between the bands resulting in a small band gap in the region between the two points at which the bands cross.

Figure 21(a) shows a cross section of the various bands of the Fermi surface of zinc by the ΓAH Brillouin zone plane. The dashed lines show the cross section of the single OPW model. The ΓA direction is equivalent to [0001] and AH is equivalent to [11$\bar{2}$0] in Fig. 20. P_3 arises from an extremal orbit around the vertical tentacle of the monster in the region where the arrow denoting the second band touches the surface. The back side of the tentacle has been drawn in from the single OPW value. This modification reduces the extremal cross-sectional area of the tentacle to fit the experimental value resulting in a surface whose shape and size fit the angular variation of P_3. This suggests that the band gap must be fairly large in the region where the monster tentacle is sucked in, and since this is the same band gap that separates the needles and the monster, seems to imply a rapid divergence of the band gap from the small value it had near K.

Thus, we have several pieces of evidence to use in forming a consistent picture. First, the effects of magnetic breakdown are quite noticeable by 1 kG, implying the existence of a very small band gap somewhere near K. Second, magnetic breakdown proceeds smoothly and rapidly and appears to be almost completed by 12 kG over a region extending 0.037 Å^{-1} above and below the ΓKM plane. This suggests a small energy gap along the entire region. Third, the bands appear to diverge rapidly when one gets 0.037 Å^{-1} above the ΓKM plane. All of these facts are consistent with a model in which the two bands cross and have two points of accidental degeneracy.

Figure 21(b) shows a cross section of this model in the region of the needle. It is assumed that the two bands cross at points 0.037 Å^{-1} above and below the ΓKM plane. The degeneracy of the bands at the point of crossing is removed by the effects of spin-orbit coupling. The energy gap will be smallest at the point of crossing, and as one goes from the crossover point toward the ΓKM plane, the energy gap will increase slowly to an extremal value in the ΓKM plane. The band gap will diverge quite rapidly in the opposite direction from the point of crossing. The effect of this is to create a region between the crossover points in which the band gap is small and nearly constant as the data seem to require.

The crossover of the bands will have a twofold effect on the geometry of the needle. First, the portion of the needle between the points of crossing will tend to be more cylindrical with a nearly constant cross section than would be the case if the bands did not cross. This might cause the needle to contribute more strongly to the de Haas–van Alphen effect than one would otherwise expect for magnetic-field directions near the hexagonal axis. Second, the surface of the needle will probably bulge out slightly near the points of crossing. This would cause a minor decrease in the de Haas–van Alphen period of the extremal orbit which passes near the bulge when the magnetic field is tilted about 80° from [0001] toward [11$\bar{2}$0]. These effects will be quite small and probably will not be observable unless the measurements are made with great precision.

CONCLUSIONS

The gross features of the galvanomagnetic properties of zinc are determined primarily by the effects of magnetic breakdown. The Fermi surface of zinc can be described quite adequately in the single zone scheme for magnetic-field strengths as large as 17 kG. Some ambiguity arises in the choice of zone scheme for $H \gtrsim 17$ kG due to the onset of magnetic breakdown across the AHL Brillouin zone plane. The breakdown does not occur across the entire plane and does not eliminate the topological openness of the monster parallel to b_3 for magnetic field strengths as large as 70 kG.

The energy gap between the monster and the needles near K is sufficiently small (about 0.01 eV) that magnetic breakdown is significant for magnetic field strengths as small as 1 kG. The gap appears to be small throughout a region extending from 0.04 Å^{-1} above the ΓKM plane to 0.04 Å^{-1} below and appears to increase quite rapidly outside of this region. This, together with certain pertinent features in the pub-

lished de Haas–van Alphen data of Joseph and Gordon, indicates that the two bands cross at a point about 0.04 Å^{-1} from the ΓKM plane.

The transition region of magnetic breakdown across the small energy gap between these two bands has been studied in detail. The quantum oscillations which are observed in the galvanomagnetic properties are a transition region phenomena resulting from a perturbation of magnetic breakdown by the Landau levels of the needle. The structure of the oscillations indicates that these Landau levels are split into discrete spin levels having a very large effective g factor. The data are insufficient at present to allow us to determine if the quasiparticle states predicted by Pippard contribute significantly to σ_{11}.

ACKNOWLEDGMENTS

The author wishes to express his sincere thanks to Dr. W. L. Gordon, Dr. M. G. Priestley, Dr. L. M. Falicov, and Dr. A. B. Pippard, F. R. S., for many stimulating and informative discussions. He is especially grateful to Dr. Pippard for communicating the results of his research prior to publication.

PHYSICAL REVIEW VOLUME 135, NUMBER 6A 14 SEPTEMBER 1964

Macroscopic Theory of Helicons*

C. R. Legéndy†

Laboratory of Atomic and Solid State Physics, Department of Physics, Cornell University, Ithaca, New York

(Received 27 April 1964)

Methods for treating boundary-value problems involving helicon waves (whistlers in solids) are developed and used for infinite plates and cylinders. The magnetoplasma inside the solid is assumed to be "driven" by means of external coils, which set up an oscillatory field with sinusoidal variation along the two coordinates tangential to the surface of the sample. The results show that in surfaces parallel to the external magnetic field an unusual surface mode is present; in this mode (for small resistivities) the power absorption due to Joule heating fails to decrease as the resistivity is decreased, until the limit of anomalous skin effect is reached, in which limit the lossy mode disappears. Several remarks are made concerning the various geometrical and physical properties of helicons.

1. INTRODUCTION

MAGNETOPLASMA oscillations obeying the same equations as atmospheric radio whistlers[1] were first reported in solids (sodium) by Bowers, Legéndy, and Rose[2]; in the context of solid-state physics they are known as *helicons*. The name is due to Aigrain,[3] who first proposed achievable experiments to detect them in solids.[4]

Sets of resonant frequencies in various materials, in addition to Na, were observed by Cotti, Wyder, and Quattropani[5,6] (In, Al, and Cu); Chambers and Jones[7] (Li, Na, K, Al, In, and InSb); Taylor, Merrill, and Bowers[8] (Cu, Ag, Au, Pb); Libchaber and Veilex[9] (InSb, at microwave frequencies); Kanai[10] (PbTe, at radio frequencies); and Khaikin, Edelman, and Mina[11] (Bi, at microwave frequencies). Detailed experimental studies of the mode structure in rectangular parallelepipeds were made by Rose, Taylor, and Bowers[12] (Na), and, with more refined detection techniques, by Merrill, Taylor, and Goodman[13] (Na). Cotti, Wyder, and Quattropani[5,6] attempted a theoretical justification for the semiempirical rule[12] obeyed by the resonant frequencies, however, the present author disagrees with their formulation of the boundary-value problem. Chambers and Jones[7] exploited the helicon resonance

* This work was supported in part by the U. S. Atomic Energy Commission.

† Present address: United Aircraft Corporation Research Laboratories, East Hartford, Connecticut.

[1] L. R. O. Storey, Phil. Trans. Roy. Soc. (London) **246A**, 113 (1953).

[2] R. Bowers, C. R. Legéndy, and F. E. Rose, Phys. Rev. Letters **7**, 339 (1961).

[3] P. Aigrain, *Proceedings of the International Conference on Semiconductor Physics, Prague, 1960* (Publishing House of the Czechoslovak Academy of Sciences, Prague, 1961), p. 224.

[4] However, see also O. V. Konstantinov and V. I. Perel', Zh. Eksperim. i Teor. Fiz. **38**, 161 (1960) [English transl.: Soviet Phys.—JETP **11**, 117 (1960)]. This article deals with electromagnetic waves in a metal, in a magnetic field. The authors apparently did not recognize the feasibility of experiments at frequencies below the collision frequency.

[5] P. Cotti, P. Wyder, and A. Quattropani, Phys. Letters **1**, 50 (1962).

[6] P. Cotti, A. Quattropani, and P. Wyder, Phys. Kondens. Materie **1**, 27 (1963).

[7] R. G. Chambers and B. K. Jones, Proc. Roy. Soc. (London) **A270**, 417 (1962).

[8] M. T. Taylor, J. R. Merrill, and R. Bowers, Phys. Rev. **129**, 2525 (1963).

[9] A. Libchaber and R. Veilex, Phys. Rev. **127**, 774 (1962).

[10] Yasuo Kanai, Japan. J. Appl. Phys. **1**, 132 (1962).

[11] M. S. Khaikin, V. S. Edel'man, and R. T. Mina, Zh. Eksperim. i Teor. Fiz. **44**, 2190 (1963) [English transl.: Soviet Phys.—JETP **17**, 1470 (1963)].

[12] F. E. Rose, M. T. Taylor, and R. Bowers, Phys. Rev. **127**, 1122 (1962).

[13] J. J. Merrill, M. T. Taylor, and J. M. Goodman, Phys. Rev. **131**, 2499 (1963).